ホームページ公開用

（様式10）
（海外特別研究員事業）

平成　30年　1月　24日

海外特別研究員最終報告書

独立行政法人 日本学術振興会 理事長　殿

採用年度　平成29年度
受付番号　222
氏　　名　望月 建爾
（氏名は必ず自署すること）

海外特別研究員としての派遣期間を終了しましたので、下記のとおり報告いたします。
なお、下記及び別紙記載の内容については相違ありません。

記

1. 用務地（派遣先国名）用務地：　ユタ大学　　　　（国名：　アメリカ　）

2. 研究課題名（和文）※研究課題名は申請時のものと違わないように記載すること。
Co-non-solvencyの分子機構

3. 派遣期間：平成　29年4月1日　～　平成29年12月26日

4. 受入機関名及び部局名
ユタ大学化学科

5. 所期の目的の遂行状況及び成果…書式任意　**書式任意（A4判相当3ページ以上、英語で記入も可）**

所期の目的の遂行状況及び成果

平成29年度採用
望月建爾

【まとめ】
本制度を利用し、ユタ大学化学科V.Molinero教授のグループに2017年4月から12月の間滞在し、共同研究を行なった。当初、メタノール水溶液中の高分子の不思議な振る舞い：共貧溶媒効果の解明を主目的とした。まず、共貧溶媒効果が原因を調べるために、球状の単純液体でも同現象が現れる事、それが排除体積効果から説明できることを明らかにした。次に、高分子が水の相転移に与える影響に興味を広げ、ポリビニルアルコールが氷の均質核生成温度を上げることを計算で再現し、さらにその分子機構の解明を行なった。高分子の不凍機能解明など、水と高分子の相互作用の研究に関してさらなる発展も期待できたが、信州大学で常勤職を得た為、9ヶ月の滞在でユタ大学を後にした。滞在中の議論から幾つかの研究テーマが浮かび、今後共同研究を行なってく予定である。短い滞在であったが、論文発表という形で研究成果をしっかり示せた。また、今後の研究に繋がる人脈作りもできたと言える。研究成果の詳細は論文として発表済みなので、以下に添付します。
【成果1】疎水分子の共貧溶媒効果
【成果2】ポリビニルアルコールが氷の均質核生成に与える影響

PCCP

COMMUNICATION

View Article Online
View Journal | View Issue

Cite this: *Phys. Chem. Chem. Phys.*, 2017, **19**, 23915

Received 20th June 2017,
Accepted 14th August 2017

DOI: 10.1039/c7cp04152g

rsc.li/pccp

Influence of co-non-solvency on hydrophobic molecules driven by excluded volume effect

Kenji Mochizuki,*[ab] Tomonari Sumi[bc] and Kenichiro Koga[bc]

We demonstrate by molecular dynamics simulation that co-non-solvency manifests itself in the solvent-induced interaction between three hydrophobes, methane, propane and neopentane, in methanol–water mixtures. Decomposition of the potential of mean force, based on the potential distribution theorem, clearly shows that the solute–solvent entropic change is responsible for stabilizing the aggregation of these hydrophobic molecules. Furthermore, we show that the entropic change pertains to the excluded volume effect.

Co-non-solvency typically refers to a situation in which a polymer is insoluble in a mixture of two solvents even though the same polymer is soluble in either one of the pure solvents. The well-known example is poly(*N*-isopropylacrylamide), PNIPAM, dissolved in methanol–water mixtures, which exhibits a re-entrant coil–globule–coil transition with the methanol concentration.[1–5] Such stimuli-responsive behaviors involving volume and solubility changes are potentially utilized for medicine and industry.[6,7] Although various explanations have been proposed,[3,8–14] the molecular origin remains a subject of debate. Very recently, Mukherji *et al.* claimed that the collapse of PNIPAM is driven by enthalpic interactions, arising from the preferential binding of methanol with PNIPAM side chains.[15–17] In contrast, van der Vegt *et al.* claimed that increases of the compressibility and the configurational entropy of collapsed PNIPAM chains caused by the preferential methanol binding are the dominant factor.[18,19] As successfully demonstrated by recent computational studies,[20–23] the preferential binding coefficients in Wyman–Tanford theory[24,25] provide the co-solvent induced shift of equilibrium constant between two different solute conformations from the view point of solvent distribution. However, this relationship does not specify which of the energetic and entropic terms in the free-energy change is dominant for the co-non-solvency effect.

Another approach for understanding the origin of co-non-solvency is to explore the minimum requirements. Mukherji *et al.* demonstrated that a generic bead-spring model can reproduce the re-entrant conformational change, regardless of specific chemical details, as long as there is a preferential energetic interaction of one of the solvents with the model polymer.[15] Yaacobi and Ben-Naim indicated, using experimental data of Ostwald absorption coefficients, that the methane–methane interaction is strengthened in ethanol–water mixtures.[26] This re-entrant change of solute–solute interaction can be regarded as a co-non-solvency effect, although we do not observe any visible clue such as clouding or liquid–liquid phase separations. The co-non-solvency effect for methane was subsequently supported by molecular dynamics (MD) simulations.[27] It was also shown that the excess chemical potential of methane monotonically decreases with the methanol concentration, although the methane–methane interaction in the mixtures exhibits a non-monotonic change. This behavior is qualitatively different from that observed for the temperature and pressure dependences.[27] Very recently, the co-non-solvency effect is also observed for tertiary butyl alcohol in methanol–water mixtures by the combination of Raman spectroscopy and MD simulations.[23]

In this communication, we investigate the potential of mean force (PMF) between a pair of three kinds of hydrophobic molecules, methane (CH_4), propane (C_3H_8) and neopentane (C_5H_{12}). Then, a decomposition of the PMF at the contact distance shows the solute–solvent entropy change, rather than the solute–solvent energy change, is responsible for the co-non-solvency effect. Furthermore, the PMF analyses for repulsive particles (or cavities) support that the entropic change pertains to the solvent excluded volume effect.

MD simulations are performed using the GROMACS 5.1.2 package.[28] TIP4P/2005 model[29] is used for water and TraPPE-UA[30–32] for the other molecules. The Lennard-Jones (LJ) parameters for cross-interactions are those given by the Lorentz–Berthelot combining rules: $\varepsilon_{ij} = \sqrt{\varepsilon_{ii}\varepsilon_{jj}}$ and $\sigma_{ij} = (\sigma_{ii} + \sigma_{jj})/2$. The Weeks–Chandler–Anderson (WCA) repulsive part[33] of the LJ solute–solvent potential is used to describe three purely repulsive particles,

---

[a] *Department of Chemistry, The University of Utah, 315 South 1400 East, Salt Lake City, Utah, 84112-0850, USA. E-mail: mochizukiborn@gmail.com*
[b] *Research Institute for Interdisciplinary Science, Okayama University, Okayama 700-8530, Japan*
[c] *Department of Chemistry, Faculty of Science, Okayama University, Okayama 700-8530, Japan*

that is cavities, which sizes are comparable to methane, propane and neopentane, respectively. The intermolecular interactions are truncated at 9.0 Å. The long-range Coulombic interactions are evaluated using the particle-mesh Ewald algorithm,[34] and dispersion corrections are implemented for the energy and pressure evaluations. To obtain PMFs between two solute molecules dissolved in 1500 solvent molecules, a set of umbrella sampling MD simulations is performed with constraining the solute–solute distance by a harmonic potential. Then, the resulting distributions of solute–solute distance are combined using the weighted histogram analysis method.[35] The computational details are described in our previous study.[36] To determine PMFs in vacuum, the similar computational procedure is used as described above. The difference is the use of constant-volume ensemble and stochastic dynamics simulations. The time step of the simulations is 2.0 fs. The production run of each umbrella sampling is 10 ns after an equilibration run of 200 ps and the configuration is recorded every 200 fs for data analyses. The pressure of 1.0 atm and temperature of T = 298 K are controlled by the Parrinello–Rahman barostat[37] and the Nosé–Hoover thermostat,[38,39] respectively, whereas the Berendsen algorithm[40] is used for equilibration. The periodic boundary conditions are applied for the cubic simulation box. To estimate the solute–solvent energy at the contact and sufficiently apart (1.4 nm) solute–solute distances, extra MD simulations of each 10 ns are performed with applying a rigid constraint to the solute–solute distance.

Fig. 1 shows PMFs for methane, propane and neopentane dimers in water, plotted against the distance r between the centers of mass. The contact distance is 0.39, 0.50 and 0.58 nm, respectively, and these distances change little with methanol concentration. Below, we focus on the influence of methanol concentration on the depth of contact minimum.

Fig. 2(a)–(c) show the PMFs at each contact distance for methane, propane and neopentane dimers as a function of methanol mole fraction x_m. The co-non-solvency effect is observed for all the solute molecules. More specifically, the PMF is lowered in the methanol–water mixtures with respect to that in either pure water or pure methanol, indicating the solute–solute interaction is strengthened in the mixtures. Comparison of the differences between PMFs at x_m = 0.0 and 0.4 (0.2 for neopentane) shows that the co-non-solvency effect becomes stronger with increasing the solute size.

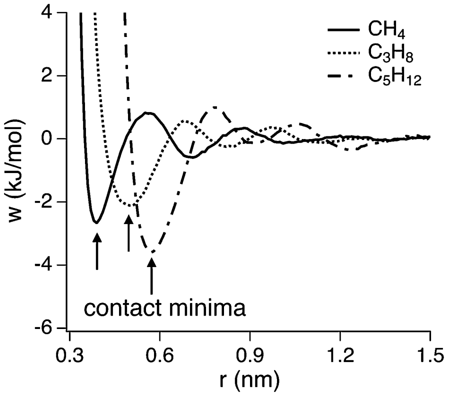

Fig. 1 Potential of mean forces w between the centers of mass (r) of methane, propane and neopentane dimers in water.

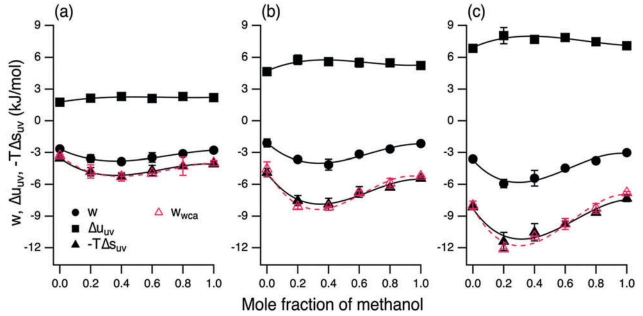

Fig. 2 Methanol mole fraction dependence of potential of mean forces (w) at each contact distance and its decomposition into solute–solvent energetic (Δu_{uv}) and entropic changes ($-T\Delta s_{uv}$) for (a) methane, (b) propane and (c) neopentane. The pink triangles are the potential of mean forces (w_{WCA}) for the corresponding solute-size cavities with WCA repulsive potential. The w_{WCA} is shifted by (a) 3.00, (b) 5.20 and (c) 7.16 kJ mol^{-1}, respectively, in order to compare the curve with that of $-T\Delta s_{uv}$.

To elucidate the driving force for the PMF reduction in methanol–water mixtures, we decompose the PMF as follows. First, on the basis of the potential distribution theorem,[41] the solute's excess chemical potential μ^*, which is the free energy change for inserting a solute into a fixed position in liquid phase (Fig. 3a), is given by

$$\mu^* = \ln\langle e^{+\delta\Psi/k_BT}\rangle_1 = \langle\Psi\rangle_1 + k_BT\ln\langle e^{+\delta\Psi/k_BT}\rangle_1 = u_{uv} - Ts_{uv} \qquad (1)$$

where k_B is the Boltzmann constant, $\langle\cdots\rangle_1$ is a conditional average taken over equilibrium configurations when the solute exists in the system, Ψ and $\delta\Psi \equiv \Psi - \langle\Psi\rangle_1$ are the solute–solvent interaction energy and the instantaneous fluctuation relative to its average value. In eqn (1), μ^* is a combination of

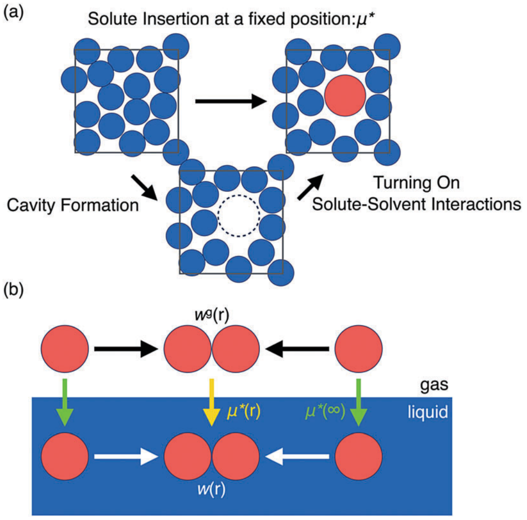

Fig. 3 Illustrations of (a) solute solvation which is divided into cavity formation and turning on solute–solvent interactions, (b) Ben-Naim's thermodynamic cycle which describes the relationship between excess chemical potential μ^* and potential of mean force w.

the average solute–solvent (uv) interaction energy $u_{\mathrm{uv}} \equiv \langle \Psi \rangle_1$, and an entropic contribution arising from fluctuations in the solute–solvent interaction energy $s_{\mathrm{uv}} \equiv -k_{\mathrm{B}} \ln[\langle e^{+\delta\Psi/k_{\mathrm{B}}T} \rangle_1]$.

According to Ben-Naim's thermodynamic cycle[42] as described in Fig. 3b, the PMF is expressed by

$$w(r) = w^{\mathrm{g}}(r) + \mu^*(r) - \mu^*(\infty) \tag{2}$$

where $\mu^*(r)$ and $\mu^*(\infty)$ are the excess chemical potentials of solute dimers which solute–solute distances are r and ∞, respectively. w^{g} is the PMF in vacuum, so that w^{g} is independent of the methanol concentration. In principle, the relative orientation between two solutes depends on the methanol concentration, and the resulting energetic and entropic changes with respect to that in gas phase are included in μ^*s of eqn (2). However, we found that these contributions are negligibly small in this study. For example, the averaged C_5H_{12}–C_5H_{12} interactions at the contact distance (r = 0.58 nm) are −3.15, −3.20, −3.18 kJ mol^{-1} in the mixtures of x_{m} = 0.0, 0.2 and 1.0, respectively.

Using eqn (1) and (2),

$$w(r) = w^{\mathrm{g}}(r) + \Delta u_{\mathrm{uv}}(r) - T\Delta s_{\mathrm{uv}}(r) \tag{3}$$

Δ denotes the changes of these quantities when the two solute molecules are brought from infinite separation to the small separation r. In this study, we use the solute–solute distance of 1.4 nm instead of the infinite separation, where two solute molecules are considered to be isolated. The $\Delta u_{\mathrm{uv}}(r)$ is directly computed by MD simulations, then the $-T\Delta s_{\mathrm{uv}}(r)$ is evaluated using eqn (3). Below, we consider only the case in which the solute–solute distance r is the contact distance of PMF, thus the expression of (r) is excluded.

Fig. 2(a)–(c) show that, for any solute, $-T\Delta s_{\mathrm{uv}}$ decreases and Δu_{uv} slightly increases with increasing x_{m} from 0 or with decreasing x_{m} from 1. The two contributions to w are mutually canceled but the change of $-T\Delta s_{\mathrm{uv}}$ is stronger and primarily determines the x_{m} dependence of w. Thus, the w reduction in the mixtures, that is the co-non-solvency effect, arises from the favorable change of $-T\Delta s_{\mathrm{uv}}$. The Δu_{uv} is positive over the entire range of x_{m}, because the solute–solvent surface area is decreased in the solute dimerization. The increase of Δu_{uv} in the mixture with respect to that in pure solvents become larger with the solute size. The decrease of $-T\Delta s_{\mathrm{uv}}$ in the mixtures is also strengthened with the solute size and the solute-size dependence is stronger than that of Δu_{uv}. Thus, the depth of w curve becomes larger with the solute size.

The results for $-T\Delta s_{\mathrm{uv}}$ give some perspectives on solvation structures. $-T\Delta s_{\mathrm{uv}}$ is expressed by $k_{\mathrm{B}}T\ln[\langle e^{+\delta\Psi/k_{\mathrm{B}}T}\rangle_1^{\alpha}/\langle e^{+\delta\Psi/k_{\mathrm{B}}T}\rangle_1^{\beta}]$, where the superscripts of α and β indicate the solute–solute distance being the contact distance and 1.4 nm, respectively. Thus, the negative value of $-T\Delta s_{\mathrm{uv}}$ indicates that the fluctuation of solute–solvent interaction energy, which results from the structural fluctuation around solutes, is suppressed in the solute dimerization. Furthermore, the $-T\Delta s_{\mathrm{uv}}$ minimum implies that such a suppression of solvation structural fluctuation is strengthened in the methanol–water mixtures.

Next, in order to investigate the origin of $-T\Delta s_{\mathrm{uv}}$, we decompose w in a different way. As described in Fig. 3a, the solute solvation can be divided into two process; (1) cavity formation and (2) turning on the solute–solvent interactions. Thus, w is also expressed by the cavity contribution w_{WCA} and the rest w_{att}; $w = w_{\mathrm{WCA}} + w_{\mathrm{att}}$.[43] The solute-size cavity is represented by the WCA repulsive potential. The pink triangles in Fig. 2 show the cavity–cavity PMFs w_{WCA} at the contact distance of w. It can be seen that the x_{m} dependence of w_{WCA} well overlaps with the $-T\Delta s_{\mathrm{uv}}$ curve in any solute. These results support that the $-T\Delta s_{\mathrm{uv}}$ change in methanol–water mixtures arises from the solvent excluded volume effect. As mentioned in the Fig. 2 caption, the w_{WCA} value is lower than the corresponding $-T\Delta s_{\mathrm{uv}}$. It is because the core size and the resulting excluded volume of WCA repulsive particle is bigger than that of LJ particle. The strengthened solvent excluded volume effect implies that a larger volume of solvation shell, or a larger number of solvated molecules, is expelled during the solute dimerization process in methanol–water mixtures than that in either one of the pure solvents.

In conclusion, our computational study shows that the co-non-solvency effect on the hydrophobic solute molecules as small as or smaller than neopentane is driven by the solute–solvent entropic change, arising from the solvent excluded volume effect. This type of effects on the hydrophobic interaction should play some role in co-non-solvency polymers because stimuli-responsive polymers commonly contain hydrophobic groups or backbones. Further investigations are required to clarify importance of each of this and other possible factors such as conformational entropy and hydrophilic interaction.

Conflicts of interest

The authors declare no competing financial interest.

Acknowledgements

This work was supported by JSPS KAKENHI Grant Numbers 15H05474, 16K05657, 26287099 and JSPS Oversea Research Fellowship. Most of the calculations were performed at the Research Center for Computational Science in Okazaki, Japan.

References

1 T. Amiya, Y. Hirokawa, Y. Hirose, Y. Li and T. Tanaka, *J. Chem. Phys.*, 1987, **86**, 2375–2379.

2 F. M. Winnik, H. Ringsdorf and J. Venzmer, *Macromolecules*, 1990, **23**, 2415–2416.

3 H. G. Schild, M. Muthukumar and D. A. Tirrell, *Macromolecules*, 1991, **24**, 948–952.

4 G. Zhang and C. Wu, *Phys. Rev. Lett.*, 2001, **86**, 822–825.

5 C. Scherzinger, A. Schwarz, A. Bardow, K. Leonhard and W. Richtering, *Curr. Opin. Colloid Interface Sci.*, 2014, **19**, 84–94.

6 M. A. Ward and T. K. Georgiou, *Polymers*, 2011, **3**, 1215–1242.

7 S. de Beer, E. Kutnyanszky, P. M. Schön, G. J. Vancso and M. H. Müser, *Nat. Commun.*, 2014, **5**, 3781.

8 J. J. Magda, G. H. Fredrickson, R. G. Larson and E. Helfand, *Macromolecules*, 1988, **21**, 726–732.

9 G. Zhang and C. Wu, *J. Am. Chem. Soc.*, 2001, **123**, 1376–1380.

10 F. Tanaka, T. Koga and F. M. Winnik, *Phys. Rev. Lett.*, 2008, **101**, 028302.

11 J. Pang, H. Yang, J. Ma and R. Cheng, *J. Phys. Chem. B*, 2010, **114**, 8652–8658.

12 J. Walter, J. Sehrt, J. Vrabec and H. Hasse, *J. Phys. Chem. B*, 2012, **116**, 5251–5259.

13 J. Dudowicz, K. F. Freed and J. F. Douglas, *J. Chem. Phys.*, 2015, **143**, 131101.

14 A. Pica and G. Graziano, *Phys. Chem. Chem. Phys.*, 2016, **18**, 25601–25608.

15 D. Mukherji, C. M. Marques and K. Kremer, *Nat. Commun.*, 2014, **5**, 4882.

16 D. Mukherji, M. Wagner, M. D. Watson, S. Winzen, T. E. de Oliveira, C. M. Marques and K. Kremer, *Soft Matter*, 2016, **12**, 7995–8003.

17 D. Mukherji, M. Wagner, M. D. Watson, S. Winzen, T. E. de Oliveira, C. M. Marques and K. Kremer, *Soft Matter*, 2017, **13**, 2292–2294.

18 F. Rodríguez-Ropero, T. Hajari and N. F. A. van der Vegt, *J. Phys. Chem. B*, 2015, **119**, 15780–15788.

19 N. F. A. van der Vegt and F. Rodríguez-Ropero, *Soft Matter*, 2017, **13**, 2289–2291.

20 J. Mondal, G. Stirnemann and B. J. Berne, *J. Phys. Chem. B*, 2013, **117**, 8723–8732.

21 J. Mondal, D. Halverson, I. T. S. Li, G. Stirnemann, G. C. Walker and B. J. Berne, *Proc. Natl. Acad. Sci. U. S. A.*, 2015, **112**, 9270–9275.

22 I. Tah and J. Mondal, *J. Phys. Chem. B*, 2016, **120**, 10969–10978.

23 K. Mochizuki, S. R. Pattenaude and D. Ben-Amotz, *J. Am. Chem. Soc.*, 2016, **138**, 9045–9048.

24 J. Wyman Jr., *Adv. Protein Chem.*, 1964, **19**, 223–286.

25 C. Tanford, *J. Mol. Biol.*, 1969, **39**, 539–544.

26 M. Yaacobi and A. Ben-Naim, *J. Solution Chem.*, 1973, **2**, 425–443.

27 K. Mochizuki and K. Koga, *Phys. Chem. Chem. Phys.*, 2016, **18**, 16188–16195.

28 M. J. Abraham, D. van der Spoel, E. Lindahl, B. Hess and the GROMACS development team, *GROMACS User Manual version 5.1.2*, 2016, www.gromacs.org.

29 J. L. F. Abascal and C. Vega, *J. Chem. Phys.*, 2005, **123**, 234505.

30 M. G. Martin and J. I. Siepmann, *J. Phys. Chem. B*, 1998, **102**, 2569–2577.

31 M. G. Martin and J. I. Siepmann, *J. Phys. Chem. B*, 1999, **103**, 4508–4517.

32 B. Chen, J. J. Potoff and J. I. Siepmann, *J. Phys. Chem. B*, 2001, **105**, 3093–3104.

33 D. Chandler, J. D. Weeks and H. C. Andersen, *Science*, 1983, **220**, 787–794.

34 T. Darden, D. York and L. Pedersen, *J. Chem. Phys.*, 1993, **98**, 10089–10092.

35 J. S. Hub, B. L. de Groot and D. van der Spoel, *J. Chem. Theory Comput.*, 2010, **6**, 3713–3720.

36 K. Mochizuki, T. Sumi and K. Koga, *Phys. Chem. Chem. Phys.*, 2016, **18**, 4697–4703.

37 M. Parrinello and A. Rahman, *J. Appl. Phys.*, 1998, **52**, 7182–7190.

38 S. Nosé, *Mol. Phys.*, 1984, **52**, 255–268.

39 W. G. Hoover, *Phys. Rev. A: At., Mol., Opt. Phys.*, 1985, **31**, 1695–1697.

40 H. J. C. Berendsen, J. P. M. Postma, W. F. van Gunsteren, A. DiNola and J. R. Haak, *J. Chem. Phys.*, 1984, **81**, 3684–3690.

41 D. Ben-Amotz, *J. Phys.: Condens. Matter*, 2016, **28**, 414013.

42 A. Ben-Naim, *Hydrophobic Interactions*, Springer, New York, 1980.

43 G. Graziano, *Chem. Phys. Lett.*, 2009, **483**, 67–71.

J|A|C|S
JOURNAL OF THE AMERICAN CHEMICAL SOCIETY

Communication

Cite This: J. Am. Chem. Soc. 2017, 139, 17003-17006

pubs.acs.org/JACS

Promotion of Homogeneous Ice Nucleation by Soluble Molecules

Kenji Mochizuki,[†,‡] Yuqing Qiu,[†] and Valeria Molinero*,[†]

[†]Department of Chemistry, The University of Utah, Salt Lake City, Utah 84112-0580, United States

[‡]Research Institute for Interdisciplinary Science, Okayama University, Okayama 700-8530, Japan

Supporting Information

ABSTRACT: Atmospheric aerosols nucleate ice in clouds, strongly impacting precipitation and climate. The prevailing consensus is that ice nucleation is promoted heterogeneously by the surface of ice nucleating particles in the aerosols. However, recent experiments indicate that water-soluble molecules, such as polysaccharides of pollen and poly(vinyl alcohol) (PVA), increase the ice freezing temperature. This poses the question of how do flexible soluble molecules promote the formation of water crystals, as they do not expose a well-defined surface to ice. Here we use molecular simulations to demonstrate that PVA promotes ice nucleation through a homogeneous mechanism: PVA increases the nucleation rate by destabilizing water in the solution. This work demonstrates a novel paradigm for understanding ice nucleation by soluble molecules and provides a new handle to design additives that promote crystallization.

Crystallization of water plays a decisive role in various fields that range from biology in subzero environments[1] and cryopreservation[2] to cloud science.[3,4] Ultrapure water droplets can be cooled to a temperature as low as 227 K,[5] where ice crystallization occurs via homogeneous nucleation, assisted only by thermal fluctuations. On the other hand, ice crystallization in nature often occurs at higher temperatures, facilitated by so-called ice nucleating agents.[6,7] Although it has long been assumed that ice nucleating agents must be insoluble substances, recent work indicates that water-soluble molecules can efficiently promote the nucleation of ice.[8]

Insoluble ice nucleating agents, such as dust, minerals, soot, and even organic monolayers, provide sufficiently large surfaces to stabilize the critical ice nuclei and promote heterogeneous ice nucleation.[9−12] Similarly, it has been proposed that soluble ice nucleating agents, such as proteins and pollen, promote ice nucleation through a heterogeneous mechanism.[8] Ice nucleation by poly(vinyl alcohol) (PVA) and a soluble polysaccharide for pollen is particularly intriguing because these molecules are expected to be highly flexible, and it has been shown that the flexibility of ice nucleating surfaces has a strong deleterious impact on ice nucleation.[9] Heterogeneous nucleation by flexible macromolecules would require their spontaneous arrangement to offer an ice-stabilizing surface, which would be penalized by a large loss of conformational entropy. Moreover, soluble molecules typically decrease the activity of water through a colligative effect, with a concomitant depression of the ice nucleation temperatures.[13,14] These issues raise the question of what is the mechanism by which soluble flexible molecules assist in the nucleation of ice.

PVA is the only fully flexible soluble ice-nucleating agent for which the molecular structure is known.[15−17] PVA increases the experimental ice crystallization temperature by up to 4 K,[15] while birch pollen polysaccharides increase it by 15−22 K.[8,18−20] It has been conjectured that the distinct ice nucleating ability of these polymers can be explained by the different dimensionality of the template they offer to stabilize ice: PVA is conjectured to serve as a 1-D template for ice nucleation, whereas the polysaccharides are proposed to act as 2-D templates.[8,15] However, a 1-D template could only stabilize a mostly 1-D ice embryo, which would have an unfavorable area to volume ratio. Interestingly, both PVA and polysaccharides of pollen exhibit both inhibition and promotion effects on ice crystallization.[15−19,21,22]

Here we use molecular simulations with computationally efficient and accurate coarse-grained models[23,24] to elucidate the molecular mechanism by which PVA nucleates ice. We first show that the simulations reproduce the experimental increase in ice nucleation temperatures by dilute PVA solutions, and then proceed to demonstrate that PVA does not heterogeneously nucleate ice, but it rather increases the homogeneous nucleation temperature through an increase in the water activity of the solution. To the best of our knowledge, this is the first demonstration that additives can increase the *homogeneous* nucleation temperature of ice.

First, we compute the effect of PVA monomer (2-propanol), 5-mer and 10-mer on the ice nucleation temperature, which we report as the freezing efficiency with respect to the homogeneous freezing temperature of pure water, $\Delta T_x = T_x^{\mathrm{solution}} - T_x^{\mathrm{water}}$, as a function of the weight percent (wt%) of PVA in the solution (Figure 1a). We find that all PVA oligomers promote ice crystallization in dilute solutions. The rise in ΔT_x for the oligomers in the simulations is independent of the molecular weight and matches the raise for the larger, 40- to 2200-mer PVA polymers in the experiments.[15] The maximum increase in freezing efficiency for the oligomers in our study, $\Delta T_x = 2.8 \pm 2$ K, is comparable to the 4 K found for the larger polymers in the experiment.[15] As in the latter,[15] the freezing efficiency decays at higher concentrations for all PVA oligomers. We find that the decrease in ΔT_x is sharper with decreasing chain length. These results demonstrate that the simulations accurately reproduce the magnitude and non-

Received: September 6, 2017
Published: November 7, 2017

DOI: 10.1021/jacs.7b09549
J. Am. Chem. Soc. 2017, 139, 17003−17006

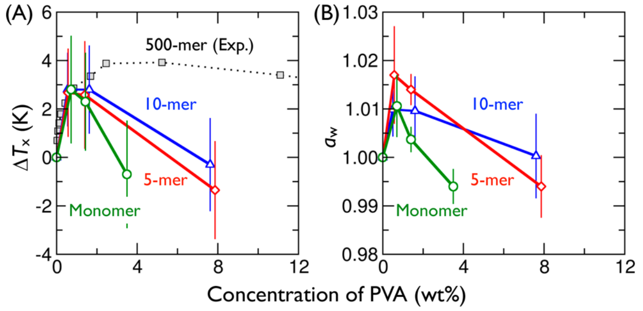

Figure 1. Freezing efficiency and water activity of PVA solutions. PVA monomer, 5- and 10-mer have a very similar effect on the ice crystallization efficiency ΔT_x, (panel A) and water activity a_w, measured at 275 K (panel B). The black dash line in panel A shows the experimental results for polydisperse PVA with molecular weight 17 600−26 400 g mol^{-1}, corresponding to 500-mer in average.[15] Panel B shows that the decline of a_w at higher PVA concentrations becomes slower with increasing chain length, a colligative effect. The activity coefficients of water in the solutions are larger than 1 for the explored concentration range (Supporting Information, Figure S4).

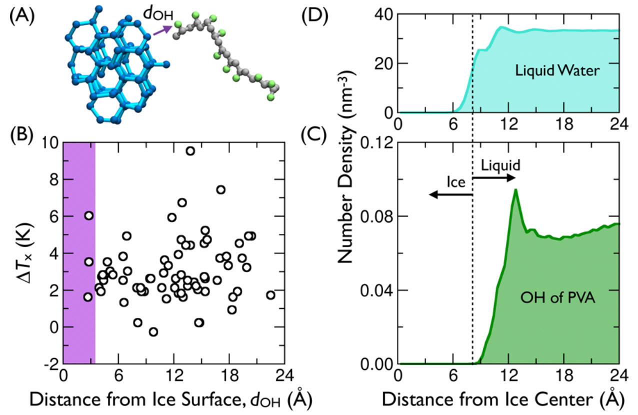

Figure 2. Ice nucleation in the presence of PVA proceeds through a homogeneous mechanism. Panel A shows snapshots of an ice embryo consisting of 81 water molecules and a PVA 10-mer. The purple arrow indicates the shortest distance (d_{OH}) from the ice embryo to the hydroxyl group (OH) of PVA. Panel B shows the freezing efficiency ΔT_x is uncorrelated to d_{OH} (obtained from 70 independent freezing trajectories, when the nucleus is of critical size, with ∼105 water molecules). We consider PVA to be absorbed to the ice embryo if its closest OH is within the first solvation shell of the water molecules in the crystal, $d_{OH} < 3.5$ Å (purple region in B). Panels C and D show equilibrium distributions of the OH of PVA and liquid water, respectively, around the constrained ice embryo consisting of 99 molecules at 275 K, plotted against the distance from center of mass of the ice embryo. The black dashed line indicates the Gibbs dividing surface between ice and water, where the surface excess of liquid water is zero (Supporting Information, part G).

monotonous concentration dependence of the ice crystallization temperature upon addition of PVA.

If ice nucleation by PVA were due to a heterogeneous mechanism, then PVA should be attached to the incipient crystalline embryo. Experimental and computational studies indicate that PVA strongly binds to the prismatic plane of ice, where it attaches in a linear, 1-D configuration.[21,24] The critical nuclei are stacking disordered[25] and small (about 100 molecules[26]); hence, they do not have well-developed prismatic faces. Indeed, 95.7% of ice nucleation events in the 0.55 wt% 10-mer solution occur without absorption of PVA to the ice crystallites. Moreover, we find no correlation between the freezing efficiency and the closest distance between PVA and the ice embryo (Figure 2a,b). We conclude that the increase in the ice freezing temperature of dilute PVA solutions cannot be attributed to heterogeneous nucleation.

This poses the question of how does PVA promote homogeneous ice nucleation. According to classical nucleation theory (CNT),[27] the nucleation rate is $J = A\exp(-\Delta G^*/k_BT)$, where A is the kinetic prefactor, ΔG^* is the free energy barrier for nucleation, k_B is the Boltzman factor, and T is the temperature. The kinetic prefactor A is only weakly dependent on T; therefore, the increase in nucleation temperature ΔT_x must be due to a decrease in the nucleation barrier ΔG^*.

The homogeneous nucleation barrier ΔG^* is controlled by the ice−liquid surface tension γ, the density of ice ρ_s and the difference in chemical potential between liquid and ice, $\Delta\mu = \mu_{\text{liquid}} - \mu_{\text{ice}}$: $\Delta G^* = 16\pi\gamma^3/(3\rho_s^2\Delta\mu^2)$. Additives that preferentially bind to the ice−liquid interface would decrease γ, thus decreasing the homogeneous nucleation barrier.[28−31] However, we find that PVA does not show preferential adsorption to the critical crystallites in the non-equilibrium nucleation trajectories (Figure 2b), nor in equilibrium simulations in which a hexagonal ice embryo is constrained to prevent its growth (Figure 2c,d). The distribution of PVA 10-mer around the ice nucleus is the same in equilibrium and non-equilibrium simulations (Supporting Information, Figure S1). This indicates that the weak adsorption of the polymer to the ice embryo is not due to dynamical effects or stacking disorder, but to the small size of the critical crystallites, which do not offer sufficient sites for adsorption of PVA to the prismatic plane. The change in ice−liquid surface tension due to the presence of PVA, $\Delta\gamma$ (Supporting Information, part G) is positive and very small, approximately 0.04 mJ m^{-2}. This would result in a small, unfavorable, +0.5% change in the free energy barrier, with minute impact on the freezing temperature. We conclude that the promotion of homogeneous nucleation by PVA is not due to a decrease in the cost of the ice−liquid interface.

The analysis above suggests that PVA increases the freezing temperature of ice through an increase in the water activity a_w of the PVA solutions. The water activity is a measure of the difference in chemical potential of pure water, μ^0_{liquid}, and water in the solution, $\mu_{\text{liquid}} = \mu^0_{\text{liquid}} + RT\ln(a_w)$. We compute a_w of PVA solutions through grand canonical molecular dynamics simulations (Supporting Information, part H),[32,33] which has been validated for the calculation of vapor pressures of bulk water,[33] nanodroplets,[34] capillary condensation in nanopores,[35] and the activity coefficients of electrolytes.[32,36] Figure 1b shows that the concentration dependence of the water activity of PVA solutions mirrors the one of ΔT_x: a_w first increases upon addition of up to about 0.6 wt% PVA, driven by repulsive non-ideal interactions with the hydrophobic moieties of PVA (Supporting Information, part I), and then decreases mostly driven by entropic, colligative effects. The increase in a_w is up to 1.1−1.7%, which corresponds to a decrease of the nucleation barrier ΔG^* from 3 to 4.6%. We conclude that small concentrations of PVA promote the homogeneous nucleation of ice through destabilization of the liquid phase.

Koop et al. demonstrated that the homogeneous nucleation temperature of ice in solutions is a function of the water activity, and independent of the nature of the solute.[13] This was validated by studies of ice nucleation in solutions of salts, organic molecules and polymers, all of which evinced a decrease

DOI: 10.1021/jacs.7b09549
J. Am. Chem. Soc. 2017, 139, 17003−17006

in freezing temperature correlated to a decrease in water activity.[13,37,38] Likewise, $\Delta T_x(a_w)$ was previously parametrized from simulations with the mW water model and a salt.[14] In all previous cases, the addition of solutes was found to decrease a_w and depress ice nucleation. Here, we show that the increase in freezing temperature of PVA solutions follows the same relation $\Delta T_x(a_w)$ derived from the salt solutions, extrapolated to $a_w > 1$ (Figure 3). The transferability of $\Delta T_x(a_w)$ across solutes implies that these do not affect the ice−liquid surface tension of the ice embryo, consistent with our analysis for PVA. There is remarkable agreement between the $\Delta T_x(a_w)$ predictions using the parametrization based on experiments[13] and simulations with mW[14] (Figure 3 and Supporting Information, Figure S6). This indicates that simulations with mW can accurately predict the effect of water activity on the freezing efficiency of solutions.

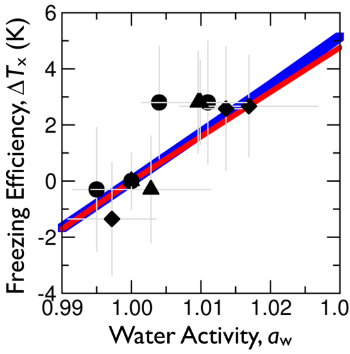

Figure 3. Ice freezing efficiency increases with the water activity of the solution. Symbols represent the simulation results for PVA solutions of monomer (circles), 5-mer (diamonds), and 10-mer (triangles). The solid lines correspond to the extrapolations of the empirical equations for $\Delta T_x(a_w)$ obtained for $a_w < 1$ from experiments of water solutions[13] (red line) and simulations of mW solutions[14] (blue line). Supporting Information, Figure S6, extends the empirical relations derived from experiments and simulations to higher water activity.

The present study demonstrates, for the first time, that ice nucleation can be promoted homogeneously through an increase of water activity, i.e., by further destabilizing the metastable liquid phase. Dilute solutions of other molecules that present hydrophobic and hydrophilic groups could, as PVA, also increase the rate of homogeneous ice nucleation. However, this effect alone might be insufficient to explain the high ice freezing efficiency measured for pollen:[18,19] Supporting Information, Figure S6, indicates that $a_w = 1.12$ would be required for $\Delta T_x = 15$ K. Solutions with such strongly non-ideal repulsive interactions may rather phase-segregate. A reduction of the ice−liquid surface tension would be required to achieve the ice nucleation potency of pollen.

We demonstrate that the prevailing paradigm for explaining promotion of ice nucleation should be expanded to include enhancement of nucleation rates through homogeneous mechanisms. Recent theoretical[29,30] and computational[30,31,39] studies of crystallization conclude that additives that reduce the surface tension of the crystal nucleus must promote homogeneous nucleation. The present study proves that additives can also promote homogeneous crystallization by destabilizing the liquid phase. This mode of action, here explored for the nucleation of ice, could also be relevant for the nucleation of clathrate hydrates of hydrophobic guests, which may also destabilize liquid water. More generally, the design of additives that destabilize the mother phase can provide a new handle for the enhancement of nucleation rates through a homogeneous mechanism.

■ ASSOCIATED CONTENT

Ⓢ Supporting Information

The Supporting Information is available free of charge on the ACS Publications website at DOI: 10.1021/jacs.7b09549.

> Models and methods, water activity coefficients, discussion of effect of hydrophobicity, and prediction of the effect of water activity on the homogeneous freezing temperature using empirical relations and classical nucleation theory (PDF)

■ AUTHOR INFORMATION

Corresponding Author

*valeria.molinero@utah.edu

ORCID

Kenji Mochizuki: 0000-0002-8947-9980
Valeria Molinero: 0000-0002-8577-4675

Notes

The authors declare no competing financial interest.

■ ACKNOWLEDGMENTS

We thank Baron Peters and Thomas Koop for insightful discussions. K.M. was supported by the Japan Society for the Promotion of Science through award 15H05474 and an oversea research fellowship. V.M. and Y.Q. were supported by the United States National Science Foundation through award CHE-1305427 "Center for Aerosol Impacts on Climate and the Environment". We acknowledge the Center of High Performance Computing at The University of Utah for technical support and an award of computing time.

■ REFERENCES

(1) Yeh, Y.; Feeney, R. E. *Chem. Rev.* **1996**, *96*, 601−618.

(2) Deller, R. C.; Vatish, M.; Mitchell, D. A.; Gibson, M. I. *Nat. Commun.* **2014**, *5*, 3244.

(3) Hiranuma, N.; Mohler, O.; Yamashita, K.; Tajiri, T.; Saito, A.; Kiselev, A.; Hoffmann, N.; Hoose, C.; Jantsch, E.; Koop, T.; Murakami, M. *Nat. Geosci.* **2015**, *8*, 273−277.

(4) Christner, B. C.; Morris, C. E.; Foreman, C. M.; Cai, R.; Sands, D. C. *Science* **2008**, *319*, 1214−1214.

(5) Sellberg, J. A.; Huang, C.; McQueen, T. A.; Loh, N. D.; Laksmono, H.; Schlesinger, D.; Sierra, R. G.; Nordlund, D.; Hampton, C. Y.; Starodub, D.; DePonte, D. P.; Beye, M.; Chen, C.; Martin, A. V.; Barty, A.; Wikfeldt, K. T.; Weiss, T. M.; Caronna, C.; Feldkamp, J.; Skinner, L. B.; Seibert, M. M.; Messerschmidt, M.; Williams, G. J.; Boutet, S.; Pettersson, L. G. M.; Bogan, M. J.; Nilsson, A. *Nature* **2014**, *510*, 381−384.

(6) Hoose, C.; Möhler, O. *Atmos. Chem. Phys.* **2012**, *12*, 9817.

(7) Murray, B.; O'sullivan, D.; Atkinson, J.; Webb, M. *Chem. Soc. Rev.* **2012**, *41*, 6519−6554.

(8) Pummer, B. G.; Budke, C.; Augustin-Bauditz, S.; Niedermeier, D.; Felgitsch, L.; Kampf, C. J.; Huber, R. G.; Liedl, K. R.; Loerting, T.; Moschen, T.; Schauperl, M.; Tollinger, M.; Morris, C. E.; Wex, H.; Grothe, H.; Pöschl, U.; Koop, T.; Fröhlich-Nowoisky, J. *Atmos. Chem. Phys.* **2015**, *15*, 4077−4091.

(9) Qiu, Y.; Odendahl, N.; Hudait, A.; Mason, R.; Bertram, A. K.; Paesani, F.; DeMott, P. J.; Molinero, V. *J. Am. Chem. Soc.* **2017**, *139*, 3052−3064.

(10) Lupi, L.; Hudait, A.; Molinero, V. *J. Am. Chem. Soc.* **2014**, *136*, 3156−3164.

(11) Marcolli, C.; Nagare, B.; Welti, A.; Lohmann, U. *Atmos. Chem. Phys.* **2016**, *16*, 8915−8937.
(12) Knopf, D. A.; Forrester, S. M. *J. Phys. Chem. A* **2011**, *115*, 5579−5591.
(13) Koop, T.; Luo, B.; Tsias, A.; Peter, T. *Nature* **2000**, *406*, 611−614.
(14) Bullock, G.; Molinero, V. *Faraday Discuss.* **2014**, *167*, 371−388.
(15) Ogawa, S.; Koga, M.; Osanai, S. *Chem. Phys. Lett.* **2009**, *480*, 86−89.
(16) Zhu, Z.; Xiang, J.; Wang, J.; Qiu, D. *Langmuir* **2017**, *33*, 191−196.
(17) Inada, T.; Koyama, T.; Goto, F.; Seto, T. *J. Phys. Chem. B* **2011**, *115*, 7914−7922.
(18) Dreischmeier, K.; Budke, C.; Wiehemeier, L.; Kottke, T.; Koop, T. *Sci. Rep.* **2017**, *7*, 41890.
(19) Pummer, B. G.; Bauer, H.; Bernardi, J.; Bleicher, S.; Grothe, H. *Atmos. Chem. Phys.* **2012**, *12*, 2541−2550.
(20) Augustin, S.; Wex, H.; Niedermeier, D.; Pummer, B.; Grothe, H.; Hartmann, S.; Tomsche, L.; Clauss, T.; Voigtländer, J.; Ignatius, K.; Stratmann, F. *Atmos. Chem. Phys.* **2013**, *13*, 10989−11003.
(21) Budke, C.; Koop, T. *ChemPhysChem* **2006**, *7*, 2601−2606.
(22) Deller, R. C.; Congdon, T.; Sahid, M. A.; Morgan, M.; Vatish, M.; Mitchell, D. A.; Notman, R.; Gibson, M. I. *Biomater. Sci.* **2013**, *1*, 478−485.
(23) Molinero, V.; Moore, E. B. *J. Phys. Chem. B* **2009**, *113*, 4008−4016.
(24) Naullage, P. M.; Lupi, L.; Molinero, V. *J. Phys. Chem. C* **2017**, DOI: 10.1021/acs.jpcc.7b10265.
(25) Lupi, L.; Hudait, A.; Peters, B.; Grünwald, M.; Gotchy Mullen, R.; Nguyen, A. H.; Molinero, V. *Nature* **2017**, *551*, 218−222.
(26) Moore, E. B.; Molinero, V. *Nature* **2011**, *479*, 506−508.
(27) Turnbull, D.; Fisher, J. C. *J. Chem. Phys.* **1949**, *17*, 71−73.
(28) Poon, G. G.; Seritan, S.; Peters, B. *Faraday Discuss.* **2015**, *179*, 329−341.
(29) Poon, G. G.; Peters, B. *J. Phys. Chem. B* **2016**, *120*, 1679−1684.
(30) Anwar, J.; Boateng, P. K.; Tamaki, R.; Odedra, S. *Angew. Chem., Int. Ed.* **2009**, *48*, 1596−1600.
(31) Duff, N.; Dahal, Y. R.; Schmit, J. D.; Peters, B. *J. Chem. Phys.* **2014**, *140*, 014501.
(32) Perez Sirkin, Y. A.; Factorovich, M. H.; Molinero, V.; Scherlis, D. A. *J. Chem. Theory Comput.* **2016**, *12*, 2942−2949.
(33) Factorovich, M. H.; Molinero, V.; Scherlis, D. A. *J. Chem. Phys.* **2014**, *140*, 064111.
(34) Factorovich, M. H.; Molinero, V.; Scherlis, D. A. *J. Am. Chem. Soc.* **2014**, *136*, 4508−4514.
(35) Factorovich, M. H.; González Solveyra, E.; Molinero, V.; Scherlis, D. A. *J. Phys. Chem. C* **2014**, *118*, 16290−16300.
(36) Lu, J.; Miller, C.; Molinero, V. *Phys. Chem. Chem. Phys.* **2017**, *19*, 17698−17707.
(37) Ganbavale, G.; Marcolli, C.; Krieger, U. K.; Zuend, A.; Stratmann, G.; Peter, T. *Atmos. Chem. Phys.* **2014**, *14*, 9993−10012.
(38) Zobrist, B.; Weers, U.; Koop, T. *J. Chem. Phys.* **2003**, *118*, 10254−10261.
(39) Poon, G. G.; Lemke, T.; Peter, C.; Molinero, V.; Peters, B. *J. Phys. Chem. Lett.* **2017**, DOI: 10.1021/acs.jpclett.7b02651.